iScience

CellPress

Article

Efficient Nitrogen Fixation Catalyzed by Gallium Nitride Nanowire Using Nitrogen and Water

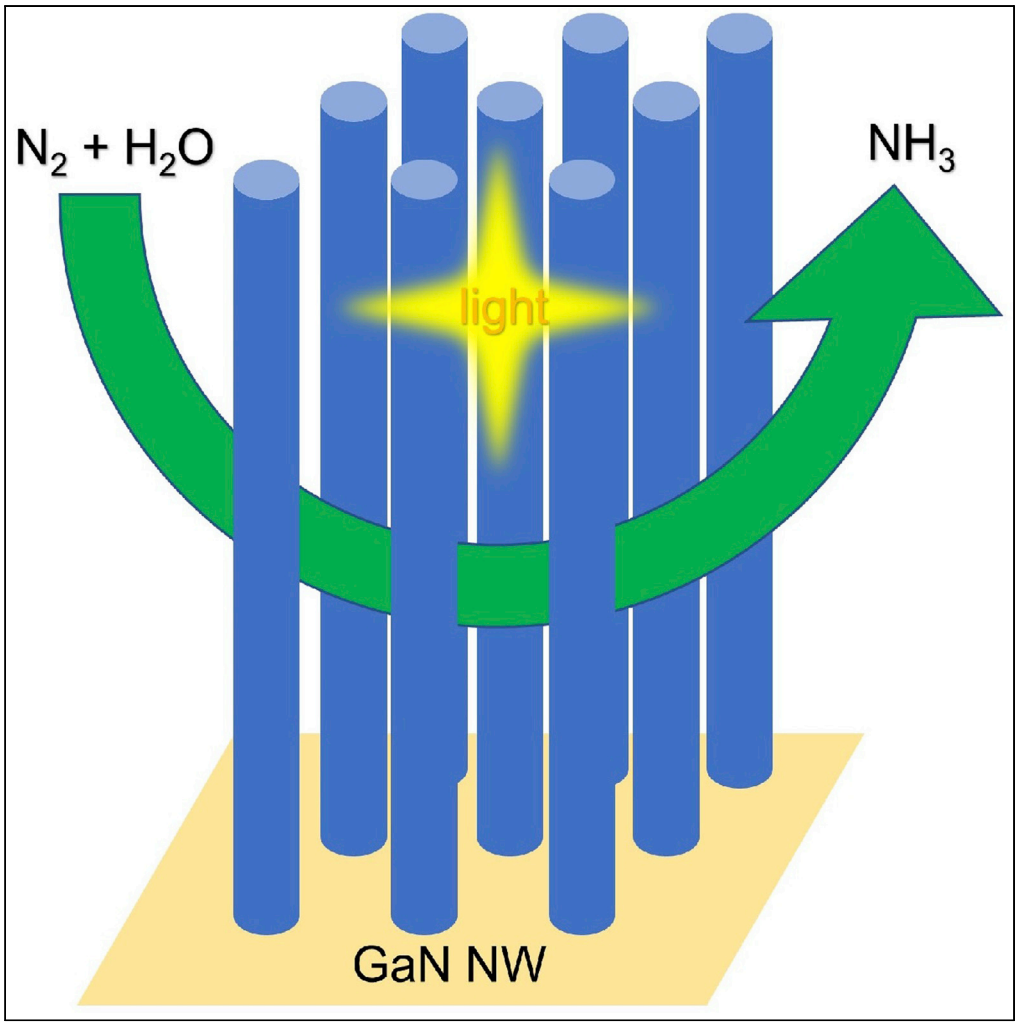

Mingxin Liu, Yichen Wang, Xianghua Kong, ..., Hong Guo, Zetian Mi, Chao-Jun Li

ztmi@umich.edu (Z.M.)
cj.li@mcgill.ca (C.-J.L.)

HIGHLIGHTS

Efficient photo-N_2 fixation

Strong chemisorption of N_2

Uses water as H source

Liu et al., iScience *17*, 208–216
July 26, 2019
https://doi.org/10.1016/j.isci.2019.06.032

iScience

CellPress

Article

Efficient Nitrogen Fixation Catalyzed by Gallium Nitride Nanowire Using Nitrogen and Water

Mingxin Liu,[1,2,7] Yichen Wang,[3,7] Xianghua Kong,[4,7] Lida Tan,[1] Lu Li,[5] Shaobo Cheng,[6] Gianluigi Botton,[6] Hong Guo,[4] Zetian Mi,[2,3,*] and Chao-Jun Li[1,8,*]

SUMMARY

Ammonia is one of the most important bulk chemicals in modern society. However, the highly energy-extensive contemporary industrial production of ammonia was developed in the early 20th century and requires extensive heating of highly pressurized flammable hydrogen gas, whose global production still relies heavily on non-sustainable petroleum. The development of "sustainable" nitrogen fixation process represents a grand aspirational chemical pursuit concerning our future human well-being. Herein, we report an ultra-stable nitride-based photosensitizing semiconductor that enables efficient, sustainable, and mild photochemical nitrogen fixation. The catalyst exhibits strong chemisorption of nitrogen and enables immediate electron donation from its surface vacancy to nitrogen. In addition, it was also demonstrated that the nitride-based semiconductor possesses the potential to minimize electron-hole recombination.

INTRODUCTION

The highly efficient and low-temperature fixation of elemental nitrogen (N_2) into ammonia (NH_3) is a highly desirable process concerning the well-being for the entire humanity. The process utilizes and transforms extremely abundant atmospheric N_2 to produce various important products such as clean fuels, fertilizers, pharmaceuticals, pesticides, explosives, dyes, bleaches, and rocket propellants (Vitousek et al., 1997). However, the stable N≡N triple bond in N_2 renders extreme chemical inertness. Up to now, the predominant method for N_2 fixation relies heavily on the Haber-Bosch process, developed a century ago, and requires harsh reaction conditions of 500°C–600°C, 20–50 MPa, and excessive flammable hydrogen (H_2) gas. Such process directly consumes more than 1% of the world's annual energy supply (Appl, 2000). Furthermore, due to the impractical energy requirement of the traditional electric water-splitting process, H_2, as the necessary feedstock for current N_2 fixation industries, is still predominantly produced from non-renewable fossil resources (Ogden, 1999). Although the development of photochemistry in recent years has been enabling N_2 fixation at ambient conditions (Chen et al., 2018), using photoexcited electrons generated from photosensitizing semiconductor catalysts such as TiO_2 (Bourgeois et al., 1988; Hirakawa et al., 2017; Hoshino, 2001; Ileperuma et al., 1990, 1993; Palmisano et al., 1988; Ranjit et al., 1996; Schrauzer and Guth, 1977; Soria et al., 1991; Zhao et al., 2014) (including its derivatives such as IIA-oxide-TiO_2 ternary compound) (Hao et al., 2016; Li et al., 1983; Oshikiri et al., 2014; Rusina et al., 2001), bismuth oxide (Bai et al., 2016; Li et al., 2015, 2016; Wang et al., 2017a, 2017b), CdS (Banerjee et al., 2015; Brown et al., 2016; Cao et al., 2016; Hu et al., 2016a, 2016b, 2016c; Khan et al., 1983; Khan and Rao, 1990; Liu et al., 2016; Miyama et al., 1980; Sun et al., 2017; Wu et al., 2013; Zhang et al., 2016), and carbonaceous materials (such as graphene (Lu et al., 2016; Yang et al., 2017), diamond (Zhu et al., 2013), and graphitic carbon nitride (Cao et al., 2017; Dong et al., 2015; Hu et al., 2016a, 2016b, 2016c, 2017; Liang et al., 2017; Wang et al., 2017a, 2017b)), still these catalysts either give highly limited N_2 conversion rate (even with large excessive N_2 flowing of >1 $L \cdot min^{-1}$) or pose stability problems and undergo photo-self-decomposition during reaction (Hoshino, 2001). Such dilemma has been keeping recent N_2 fixation researches from gaining further practical impact. Therefore, an innovative design that offers the solution and inspires the potential photo-fixation advancement toward a more sustainable future remains highly desirable.

Ever since the first single-crystalline growth in 1969 (Maruska and Tietjen, 1969), nitride semiconductors, represented by gallium nitride (GaN), have attracted much research attention for their extreme stability (melting point >2,500°C), which at the same time enables more than six magnitudes of voltage carrying

[1]Department of Chemistry and FRQNT Centre for Green Chemistry and Catalysts, McGill University, 801 Sherbrooke Ouest, Montreal, QC H3A 0B8, Canada

[2]Department of Electrical Engineering and Computer Science, University of Michigan, 1301 Beal Avenue, Ann Arbor, MI 48109, USA

[3]Department of Electrical and Computer Engineering, McGill University, 3480 University, Montreal, QC H3A 0E9, Canada

[4]Department of Physics, McGill University, Rutherford Building, 3600 University, Montreal, QC H3A 2T8, Canada

[5]State Key Laboratory of Inorganic Synthesis and Preparative Chemistry, Chemistry Department, Jilin University, Changchun, China

[6]Department of Material Science and Engineering, Canadian Centre for Electron Microscopy, McMaster University, 1280 Main Street West, Hamilton, ON L8S 4M1, Canada

[7]These authors contributed equally

[8]Lead Contact

*Correspondence: ztmi@umich.edu (Z.M.), cj.li@mcgill.ca (C.-J.L.)

https://doi.org/10.1016/j.isci.2019.06.032

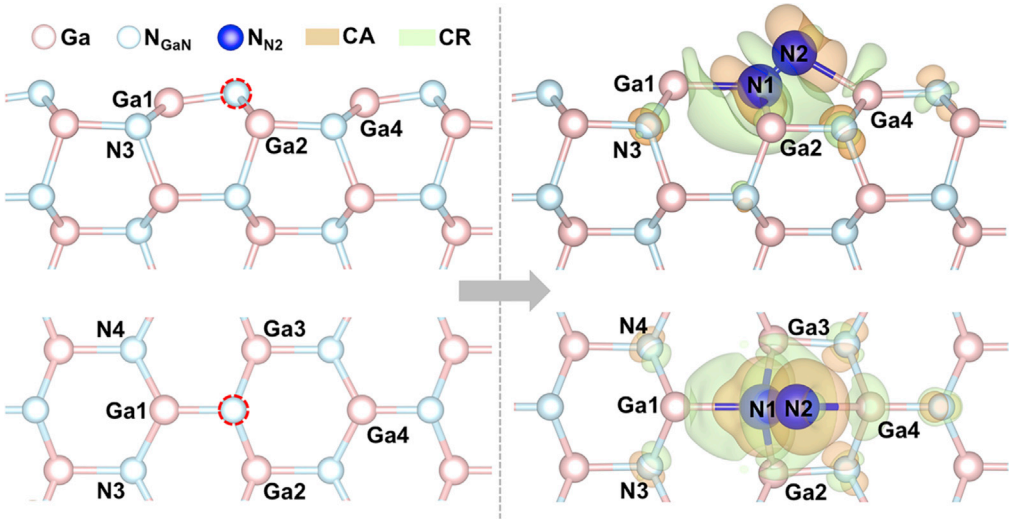

Figure 1. Geometric and Electronic Properties of N_2 Adsorption on GaN (10 $\bar{1}$0)-Wurtzite with N Vacancy

(Left) Top (upper) and side (bottom) views of the fully relaxed atomic structures of GaN (10 $\bar{1}$0)-wurtzite. The position of N vacancy is marked with red dashed circle. (Right) Top (upper) and side (bottom) views of the fully relaxed atomic structures and differential charge density of N_2 adsorption on GaN (10 $\bar{1}$0)-wurtzite with N vacancy. CA indicates charge accumulation, whereas CR represents charge reduction. Isosurface contours of electron density differences are drawn at $\pm$0.002 e·Å^{-3}; see also Figure S4 and Table S3.

enhancement and dissipation inhibition compared with conventional oxide semiconductors (Pearton, 1997). With those superior properties, the nitride semiconductor is believed to serve as the semiconductor of the future (Akasaki, 2002). We have demonstrated the superior performance of GaN and its derivatives to carry out highly efficient catalytic photo-water-splitting (Fan et al., 2015; Kibria et al., 2016; Wang et al., 2011; Xu et al., 2018). In early 2017, we reported the preliminary results about GaN as an efficient photosensitizer to conduct ruthenium(Ru)-catalyzed photochemical N_2 fixation, which achieved record catalytic conversion rate (Li et al., 2017). Nevertheless, the rate per gram of catalyst was still limited. In addition, the fixation still requires the flammable and non-sustainable H_2 gas as the reductant with scarce noble metal as the catalyst. We then contemplated the feasibility to eliminate the use of hydrogen by using water as reductant to conduct highly efficient GaN-catalyzed N_2 fixation. Herein, we would like to report photochemical N_2 fixation using only N_2 and water catalyzed by GaN nanowire (NW).

RESULTS AND DISCUSSIONS

Design and Density Functional Theory Calculation

The initial donation of an electron to the ground-state N_2 ($N_2 + e^- \rightarrow N_2^-$) serves as the rate-limiting step of the entire N_2 fixation into NH_3 (Bauer, 1960). However, a large reduction potential of −4.2 V (versus normal hydrogen electrode) poses significant energy barrier. As an initial design, we envisioned that such energy barrier might be easily reduced by using materials that adsorb N_2 on its surface and stabilize the generated N_2^- intermediate ($N_{2\,(gas)} + e^- + \text{material} \rightarrow N_2^-{}_{(adsorbed)}$). The GaN NW was then chosen for its high surface activity and stability to serve as an ideal platform to test our hypothesis. We first performed systematic density functional theory (DFT) calculations to test the N_2 adsorption characteristics on GaN NW surface (Figure 1, see Supplemental Information for calculation details). The calculation showed that the N_2 molecules adsorb on the pristine GaN surfaces via physisorption. However, N vacancies, which have been suggested by many reports on epitaxially grown GaN surface even without further defect engineering process (Moustakas and Molnar, 1992; Kaufmann et al., 2000; Neugebauer and van de Walle, 1996; Hautakangas et al., 2003; Newman, 1997), can potentially enable strong chemisorption of N_2. Illustrated in Figure 1, for the surfaces with N vacancies marked with red dashed circles, the N_2 molecule prefers to adsorb at the vacancy site. One N atom (N1) attaches to the Ga atom (Ga1) with bond length of 2.27 Å as well as Ga2 and Ga3 atoms with a shorter bond length of 2.07 Å. The other N atom (N2) approaches the Ga atom (Ga2) of the adjacent dimer across the dimer row with a bond length of 2.23 Å. Such a strong bonding between N_2 and the GaN surface results in an elongated bond length of N_2 from the original 1.11 to 1.28 Å. The

weakened N1-N2 bonds suggest a significant activation of N_2 molecules upon chemisorption on the GaN surface with N vacancies. Differential charge density was plotted on the right side of Figure 1 to understand the bonding mechanism between N_2 and the GaN surface. There is a significant charge accumulation (indicated by the light orange color) around the nitrogen antibonding orbital and charge reduction (indicated by the light green color) near the Ga atoms. This implies electron donation from Ga to the antibonding orbital of N_2 and an ionic-like Ga-N bonding. In addition, for the N_2 molecule itself, substantial charge reduction was found between the N1-N2 bonds, which also contributes to the reason that the N1-N2 bonds are weakened and elongated significantly. As a consequence, the charge transfer activates the N_2 molecule upon the adsorption on GaN with N vacancies. The results of Bader charge analysis (Henkelman et al., 2006; Bader, 1985) before and after the adsorption provide a quantitative description of the charge changes (see Figure S4 and Table S3). Impressively, the N_2 molecule (in Figure 1) exhibited an electronegativity of 1.1080 e, in which N1 and N2 atoms obtained 0.7582 e and 0.3498 e, respectively, from the substrate (see Table S3). This indicates that one electron has been donated from GaN to N_2 upon its adsorption on the N vacancy of GaN, giving the critical N_2^- intermediate. With light irradiation, this intermediate should be further reduced rapidly toward NH_3 by photoexcited electrons from GaN.

Photo-Driven Nitrogen Fixation with Gallium Nitride Nanowire

With the positive computational results, we began to grow the GaN NW by plasma-assisted molecular beam epitaxy on commercially available Si(111) wafer. The scanning electron microscopic result in Figure 2A clearly shows the NW arrays aligning vertically to the wafer. The transmission electron microscopic (TEM) result of a single NW demonstrates its size to be approximately 50–80 nm in diameter and 800 nm in height. We also used Si and Mg doping to generate the corresponding n- and p-type GaN NWs, as those dopants can significantly vary the semiconductor's surface Fermi level, band bending, etc. Adapted from our previous report (Kibria et al., 2013), InGaN segment was also incorporated to the GaN NWs (InGaN/GaN) to examine the catalytic conversion rate under visible light.

The synthesized GaN NW was examined as the catalyst toward photochemical N_2 fixation using water in a 425-mL sealed quartz reactor under light illumination for 1 h (see Transparent Methods or Figure S1 in Supplemental Information for detail). To our delight, p-GaN NW gave 190 $\mu mol \cdot g_{cat}^{-1} \cdot h^{-1}$ catalytic conversion rate toward NH_3 (Figure 2B). Using the same deposition protocol, i-GaN NW gave 310 $\mu mol \cdot g_{cat}^{-1} \cdot h^{-1}$ rate. n-GaN NW gave an astonishing 450 $\mu mol \cdot g_{cat}^{-1} \cdot h^{-1}$ rate. Commercially available GaN powder gave a reduced rate of 170 $\mu mol \cdot g_{cat}^{-1} \cdot h^{-1}$. It was shown that the reaction did not give any product in dark. We also examined our reaction under visible light using a long-pass filter (>400 nm) applied to the light source under the same reaction conditions. It was shown that under this condition, the previously optimized n-GaN NW only gave a trace amount of product, whereas n-InGaN/GaN NW gave 340 $\mu mol \cdot g_{cat}^{-1} \cdot h^{-1}$ catalyst conversion rate. With the optimized catalyst in hand, we attempted to increase the NH_3 yield by prolonging the reaction time. However, the prolonged reaction time did not give significant increase in NH_3 yield (see Table S1), possibly due to the strong adsorption of NH_3 on GaN surface. We then attempted to recycle the used catalyst and repeat the reaction cycle with freshly loaded N_2 and distilled water. Surprisingly, the catalyst exhibited potent activity even after 13 consecutive cycles, with no further treatment applied to re-activate the catalyst between each cycle (Figure 2C, see also Figures S8–S10, Supplemental Information for detailed result of each cycle). The combined NH_3 yield reaches 5,700 $\mu mol \cdot g_{cat}^{-1}$. Providing the overall reaction Gibbs free energy change $\Delta G = +339$ kJ/mol (Thacker et al., 1941) and the total power input E = 300 W × 3,600 s × 13, the overall energy efficiency was an astonishing $N_{NH3} \cdot \Delta G \cdot E^{-1} \times 100\% = 5\%$. To confirm the origin of nitrogen in the generated NH_3, ^{15}N isotope labeling experiment was conducted. We first conducted the previously optimized reaction using $^{15}N_2$ (98% purity, purchased from Aldrich) instead of the normal ultra-high-purity $^{14}N_2$ with GaN grown under normal $^{14}N_2$. To our surprise, $^{14}NH_3$ was still generated as the main product (Figure 2D). It was not until the catalyst evacuated at high temperature and vacuum (>400°C under $<5 \times 10^{-2}$ mbar for 12 h) before the reaction that $^{15}NH_3$ prevailed as the main product, indicating that the $^{14}NH_3$ product was mainly from the adsorption of atmospheric N_2 to the catalyst, and not from GaN decomposition. Intriguingly, this result shows an extraordinarily great adsorption tendency for N_2 on GaN NW surface, which is consistent with our initial DFT studies. To further examine the surface property of the GaN NW, electron paramagnetic resonance (EPR) study was conducted for the freshly synthesized catalyst sample (Figure 2E). The detection of a resonance peak at approximately 3,450 G is consistent with previous reports (Palczewska et al., 1998; Nonomura et al., 1996; Carlos et al., 1993) and therefore confirms the presence of vacancy defect. In addition, a much less significant EPR signal was obtained after treating the catalyst with N_2, indicating the interaction of the vacancy defect with N_2. Furthermore, a temperature

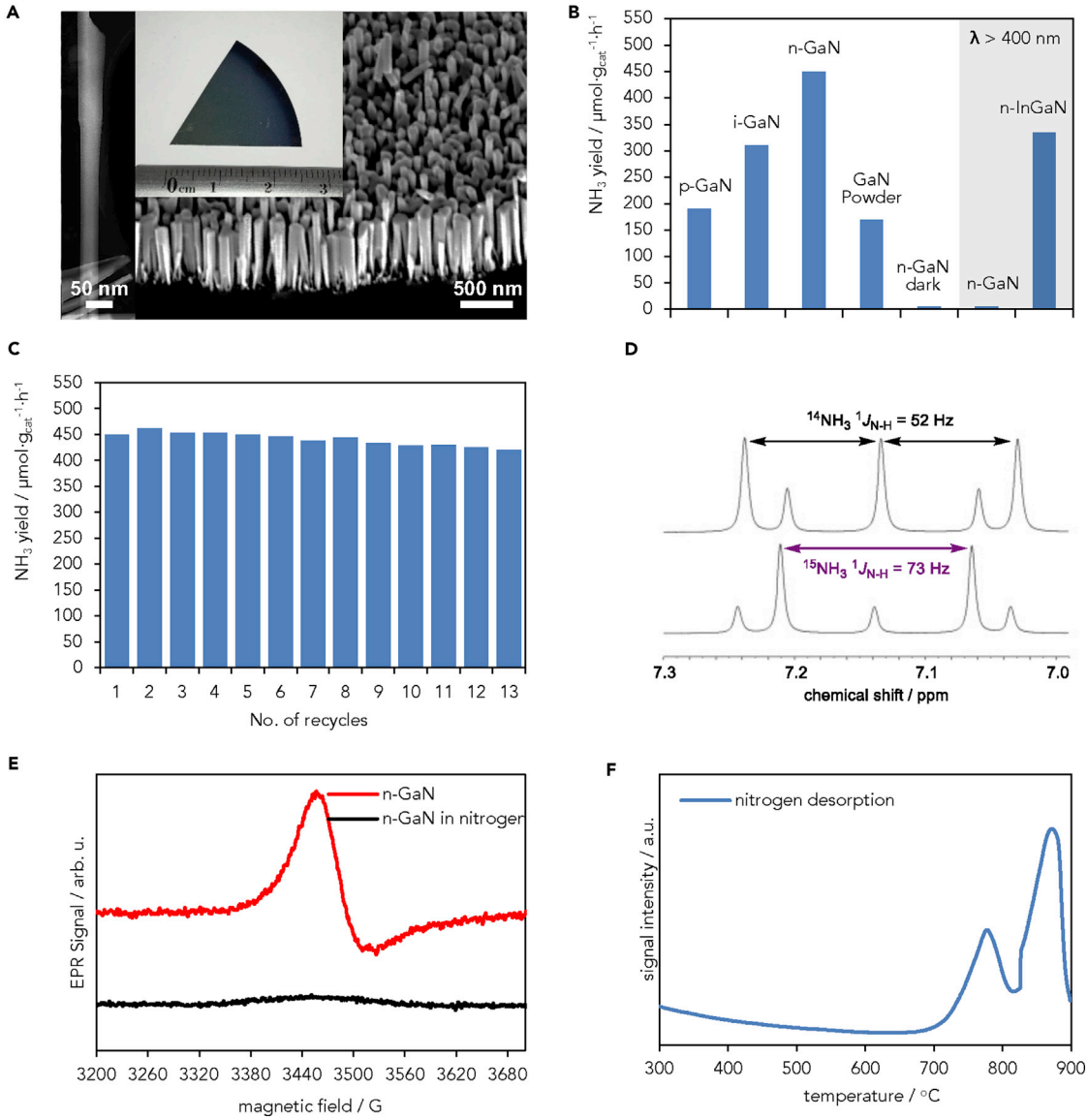

Figure 2. Photochemical N_2 Fixation Results

(A) Microscopic identification of the GaN NW catalyst; (left) Transmission Electron Microscopy Image; (right) scanning electron microscopic image; inset, catalyst slice seen by the naked eye.

(B) GaN NW with different dopants under light illumination and with >400-nm filter, See also Table S1.

(C) n-GaN catalyst recyclability test, See also Table S1.

(D) ^{15}N-labeling experiment result before (above) and after (below) removing adsorbents on the catalyst.

(E) EPR spectrum of the freshly synthesized and N_2-treated n-GaN NW catalyst, acquired with microwave power of 20 dB at room temperature.

(F) Temperature programmed desorption of N_2 on n-GaN NW.

programmed desorption (TPD) study was conducted using freshly synthesized n-GaN NW (Figure 2F), which was placed under N_2 at 45°C for 2 h before TPD. The result clearly shows evidence for N_2 chemisorption of n-GaN NW surface and the accuracy of our DFT predictions. To examine the possibility for GaN decomposing, X-ray photoelectron spectrum was collected for the GaN NW before and after the reaction, showing the exact same binding energy on Ga^{3d} band (see Figure S5), therefore indicating no decomposition in GaN.

Effect of Ruthenium Deposition and the Selectivity Shift

To see if the N_2 fixation efficiency can be further enhanced by incorporating the GaN NW with co-catalyst such as ruthenium nanoparticle (Ru NP), which can significantly enhance the GaN-catalyzed N_2 fixation

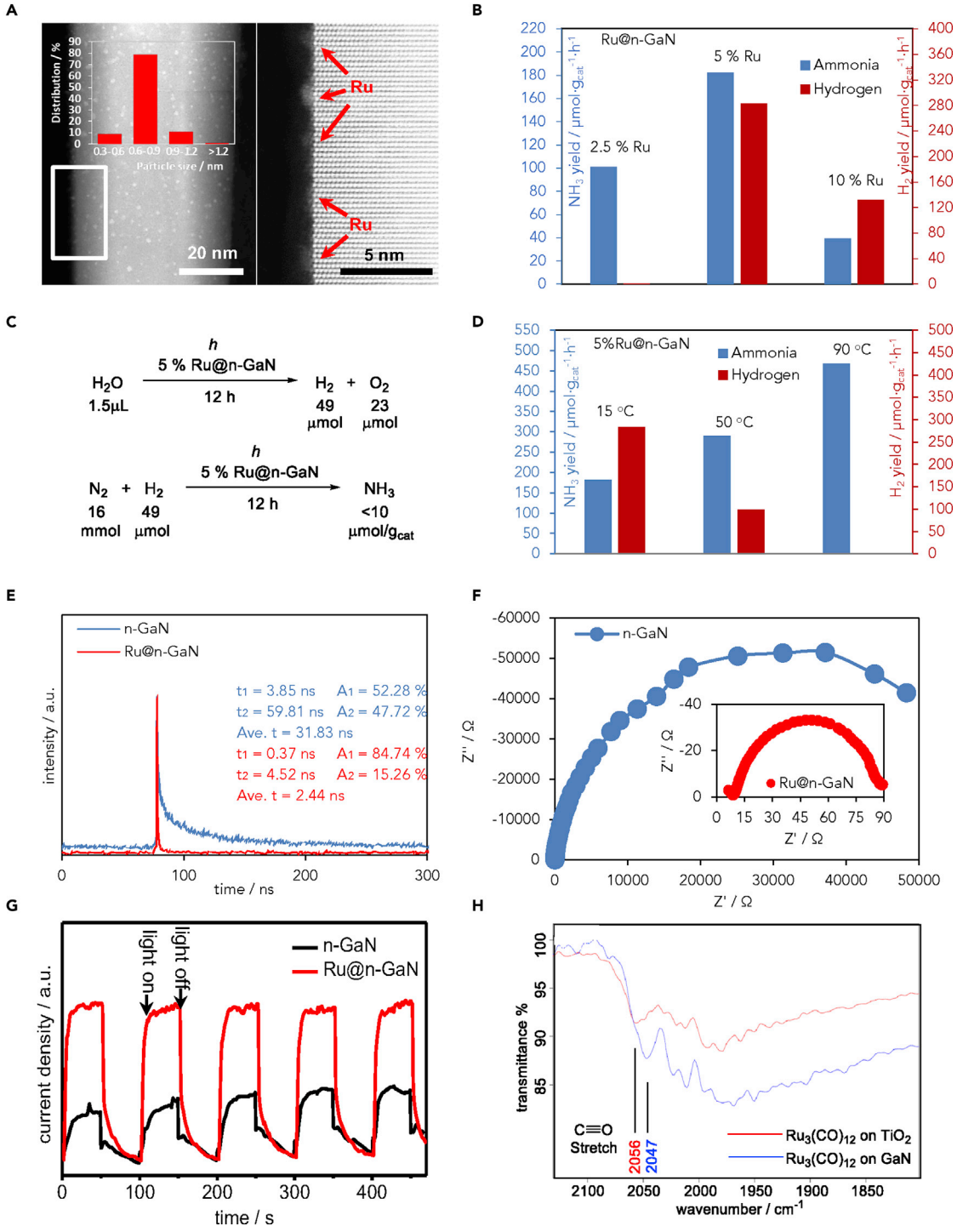

Figure 3. Photo-production of Ammonia and Hydrogen by Ru@GaN and Characterization

(A) TEM identification of Ru@GaN NW; right image shows the zoom-in region of the square area of the left image, showing Ru NP; inset, particle size distribution.

(B) N_2 fixation and HER results of Ru@n-GaN catalyst with different Ru loads, See also Table S2.

(C) Control experiments without N_2 and with H_2, See also Table S2.

(D) Temperature-controlled selectivity change for Ru@n-GaN NW, See also Table S2.

(E) Time-resolved photoluminescence result for n-GaN NW and Ru@n-GaN NW.

Figure 3. *Continued*

(F) Electrochemical impedance spectra of n-GaN NW and Ru@n-GaN NW (inset).

(G) Transient photocurrent spectra of n-GaN NW and Ru@n-GaN NW.

(H) IR spectra for the carbonyl region of $Ru_3(CO)_{12}$@GaN and $Ru_3(CO)_{12}$@TiO_2, see also Figure S7.

under H_2 by generating unique metal/semiconductor interfacial Schottky junction (Li et al., 2017), the incorporation of Ru was done by impregnating GaN NWs with a dilute solution of $Ru_3(CO)_{12}$ followed by gradually heating under vacuum to liberate the solvent and carbonyls (see Transparent Methods and Figures S2 and S3 in Supplemental Information for experimental details). The presence of Ru NP on GaN NW surface was confirmed by TEM result (Figure 3A), as extremely small clusters of <1 nm size even with 5 wt % Ru loading (versus GaN). However, the GaN-catalyzed N_2 fixation by water gave vastly different results compared with our previous N_2 fixation by H_2, as the incorporation of Ru NP decreased the N_2 fixation efficiency, whereas the hydrogen evolution reaction (HER) was greatly promoted by the generation of excessive H_2 with Ru load reaching 5 wt % and over versus GaN (Figure 3B). This indicated that the Ru NP, although enriched with e^- by the metal/semiconductor Schottky junction, (Li et al., 2017) serves as the site for HER rather than N_2 fixation, which is less energetically favored than HER (see Figure S6 for a proposed energy diagram). This is also consistent with our knowledge that GaN-catalyzed water splitting can be promoted by the incorporation of noble metal, which serves as the site for HER by donating photoexcited e^- to H^+ (Fan et al., 2015; Kibria et al., 2016; Wang et al., 2011; Xu et al., 2018). As the same Ru@GaN catalyst giving 49 μmol hydrogen in the water-splitting test (note that no NH_3 is detected, Figure 3C), N_2 fixation control experiment with 49 μmol hydrogen instead of water also gave only negligible conversion rate, indicating that NH_3 was unlikely to be synthesized from *in situ*-generated hydrogen in Ru@GaN-catalyzed N_2 fixation by water. To further examine this process, parallel experiments were conducted using 5 wt % Ru@GaN under elevated temperature (Figure 3D). Increased N_2 fixation selectivity was observed as the temperature rises, with almost complete selectivity observed when the reaction was conducted at 90°C. This indicated that the N_2 fixation selectivity rises with enhanced thermal motion of carrier at elevated temperature, which inhibits photoexcited e^- transfer from GaN and its vacancy, the suggested N_2 fixation site, to Ru NP, the suggested HER site. To further examine the e^- transfer from GaN to Ru, time-resolved photoluminescence spectra were recorded for n-GaN NW and Ru@n-GaN NW at room temperature. The average emission lifetime of Ru@n-GaN (2.44 ns) was significantly reduced compared with that of n-GaN (31.83 ns) (Figure 3E). Electrochemical impedance spectra (EIS) for n-GaN and Ru@n-GaN also showed a greatly reduced semicircle in Nyquist plots for Ru@n-GaN compared with n-GaN (Figure 3F). Transient photocurrent spectra for the same catalysts again showed enhanced photocurrent for Ru@n-GaN (Figure 3G). These evidences clearly show the significant carrier-transfer from GaN NW to Ru NP at room temperature. Such efficient carrier-transfer is scarce among most photosensitizing semiconductors, as carrier-recombination is common and significant, especially for predominantly studied oxide-based semiconductors (Comer et al., 2018). Infrared (IR) spectra of $Ru_3(CO)_{12}$@GaN and $Ru_3(CO)_{12}$@TiO_2 clearly show a higher wave number for carbonyl stretch on TiO_2 compared with GaN (Figure 3H, see Figure S7 for full IR spectra), indicating a stronger electron withdrawing on Ru by TiO_2 compared with by GaN, and hence a greater tendency for carrier-recombination for Ru@TiO_2 compared with Ru@GaN.

Conclusion

In summary, we have demonstrated the ability of GaN NW as a powerful heterogeneous catalyst for photochemical N_2 fixation by water. We have demonstrated that the surfaces with N vacancy of wurtzite GaN NW photocatalysts are highly reactive with N_2 molecules and offer unique advantages for N_2 photoreduction. Different from GaN-catalyzed N_2 fixation by H_2, the incorporated Ru NP decreased the efficiency of GaN-catalyzed N_2 fixation by water, possibly by serving as the center for HER. We also demonstrated the ability for GaN as a nitride-based semiconductor to inhibit electron-hole recombination steps. Further development of the GaN NW as a photochemical nitrogen fixation catalyst toward more practical and industrialized process is already underway in our laboratory.

Limitations of Study

Owing to the limited experimental conditions and equipment, we were unable to test the direct growth of GaN NW inside the inner wall of large-scale reaction vessel. This experiment can bring the reported N_2 photo-fixation closer to industrialization, which is an appealing and highly interesting examination if successfully conducted.

METHODS

All methods can be found in the accompanying Transparent Methods supplemental file.

SUPPLEMENTAL INFORMATION

Supplemental Information can be found online at https://doi.org/10.1016/j.isci.2019.06.032.

ACKNOWLEDGMENTS

M.L. and C.-J.L. are grateful to the Canada Research Chair (Tier 1) Foundation, the Natural Sciences and Engineering Research Council of Canada, Fonds de Recherche du Québec - Nature et Technologies, Canada Foundation for Innovation (CFI), and McGill University for financial support. M.L. is also grateful for L.L.'s help and suggestions, Dr. Robin Stein's kind assistance in NMR and EPR analyses, and the help from Ms. Alicia Junqi Wu, Dr. Timothy Mack, and Prof. Mark Andrew for the PL measurement. Y.W. and Z.M. are grateful for Emission Reduction Alberta for funding. X.K. and H.G. acknowledge financial support of the Natural Science and Engineering Research Council of Canada and thank Compute Canada and the High-Performance Computing Center of McGill University for computation facilities. L.T. would like to thank Mr. Kanchan Dutta and Prof. Jan Kopyscinski for the help in TPD measurement.

AUTHOR CONTRIBUTIONS

M.L. was responsible for designing and carrying out all the necessary experiments except for the MBE growth and the computational studies. He was also in charge of conceiving the concept of the research and composing the manuscript for publication. Y.W. was responsible for designing the NW synthesis, operating the MBE device, and provide technical help. X.K. and H.G. participated in crucial discussions and completed the computational studies. L.T. participated in crucial discussions and designed the TPD experiment. S.C. and G.B. completed the microscopic identification of the catalyst. L.L. provided some valuable suggestions. General guidance and overall project directing was done by Z.M. and C.-J.L.

DECLARATION OF INTERESTS

The authors declare no competing financial interests.

Received: November 21, 2018
Revised: April 26, 2019
Accepted: June 23, 2019
Published: July 26, 2019

REFERENCES

Akasaki, I. (2002). Nitride semiconductors – impact on the future world. J. Cryst. Growth *237-239*, 905–911.

Appl, M. (2000). Ullmann's Encyclopedia of Industrial Chemistry (Wiley-VCH Verlag GmbH and Co. KGaA).

Bader, R.F.W. (1985). Atoms in molecules. Acc. Chem. Res. *18*, 9–15.

Bai, Y., Ye, L., Chen, T., Wang, L., Shi, X., Zhang, X., and Chen, D. (2016). Facet-dependent photocatalytic n_2 fixation of bismuth-rich bi5o7i nanosheets. ACS Appl. Mater. Interfaces *8*, 27661–27668.

Banerjee, A., Yuhas, B.D., Margulies, E.A., Zhang, Y., Shim, Y., Wasielewski, M.R., and Kanatzidis, M.G. (2015). Photochemical nitrogen conversion to ammonia in ambient conditions with FeMoS-chalcogels. J. Am. Chem. Soc. *137*, 2030–2034.

Bauer, N. (1960). Theoretical pathways for the reduction of N2 molecules in aqueous media: thermohynamics of N_2H_n. J. Phys. Chem. *64*, 833–837.

Bourgeois, S., Diakite, D., and Perdereau, M. (1988). A study of titanium(IV) oxide powders as a support for the photochemical synthesis of ammonia. React. Solids *6*, 95–104.

Brown, K.A., Harris, D.F., Wilker, M.B., Rasmussen, A., Khadka, N., Hamby, H., Keable, S., Dukovic, G., Peters, J.W., Seefeldt, L.C., and King, P.W. (2016). Light-driven dinitrogen reduction catalyzed by a CdS:nitrogenase MoFe protein biohybrid. Science *352*, 448–450.

Cao, Y., Hu, S., Li, F., Fan, Z., Bai, J., Lu, G., and Wang, Q. (2016). Photofixation of atmospheric nitrogen to ammonia with a novel ternary metal sulfide catalyst under visible light. RSC Adv. *6*, 49862–49867.

Cao, S., Zhou, N., Gao, F., Chen, H., and Jiang, F. (2017). All-solid-state Z-scheme 3,4-dihydroxybenzaldehyde-functionalized Ga_2O_3/graphitic carbon nitride photocatalyst with aromatic rings as electron mediators for visible-light photocatalytic nitrogen fixation. Appl. Catal. B *218*, 600–610.

Carlos, W.E., Freitas, J.A., Jr., Asif Khan, M., Olson, D.T., and Kuznia, J.N. (1993). Electron-spin-resonance studies of donors in wurtzite GaN. Phys. Rev. B *48*, 17878–17884.

Chen, X., Li, N., Kong, Z., Ong, W.-J., and Zhao, X. (2018). Photocatalytic fixation of nitrogen to ammonia: state-of-the-art advancements and future prospects. Mater. Horiz. *5*, 9–27.

Comer, B.M., Liu, Y.-H., Dixit, M.B., Hatzell, K.B., Ye, Y., Crumlin, E.J., Hatzell, M.C., and Medford, A.J. (2018). The role of adventitious carbon in photo-catalytic nitrogen fixation by titania. J. Am. Chem. Soc. *140*, 15157–15160.

Dong, G., Ho, W., and Wang, C. (2015). Selective photocatalytic N_2 fixation dependent on g-C_3N_4 induced by nitrogen vacancies. J. Mater. Chem. A *3*, 23435–23441.

Fan, S., AlOtaibi, B., Wang, Y., Mi, Z., Woo, S.Y., Botton, G.A., and Mi, Z. (2015). High efficiency solar-to-hydrogen conversion on a monolithically integrated InGaN/GaN/Si adaptive tunnel junction photocathode. Nano Lett. *15*, 2721–2726.

Hao, Y., Dong, X., Zhai, S., Ma, H., Wang, X., and Zhang, X. (2016). Hydrogenated bismuth molybdate nanoframe for efficient sunlight-driven nitrogen fixation from air. Chem. Eur. J. *22*, 18722–18728.

Hautakangas, S., Oila, J., Alatalo, M., Saarinen, K., Liszkay, L., Seghier, D., and Gislason, H.P. (2003). Vacancy defects as compensating centers in Mg-doped GaN. Phys. Rev. Lett. *90*, 137402.

Henkelman, G., Arnaldsson, A., and Jonsson, H. (2006). A fast and robust algorithm for Bader decomposition of charge density. Comp. Mater. Sci. *36*, 354–360.

Hirakawa, H., Hashimoto, M., Shiraishi, Y., and Hirai, T. (2017). Photocatalytic conversion of nitrogen to ammonia with water on surface oxygen vacancies of titanium dioxide. J. Am. Chem. Soc. *139*, 10929–10936.

Hoshino, K. (2001). New avenues in dinitrogen fixation research. Chem. Eur. J. *7*, 2727–2731.

Hu, S., Chen, X., Li, Q., Zhao, Y., and Mao, W. (2016a). Effect of sulfur vacancies on the nitrogen photofixation performance of ternary metal sulfide photocatalysts. Catal. Sci. Technol. *6*, 5884–5890.

Hu, S., Li, Y., Li, F., Fan, Z., Ma, H., Li, W., and Kang, X. (2016b). Construction of g-C_3N_4/$Zn_{0.11}Sn_{0.12}Cd_{0.88}S_{1.12}$ hybrid heterojunction catalyst with outstanding nitrogen photofixation performance induced by sulfur vacancies. ACS Sustain. Chem. Eng. *4*, 2269–2278.

Hu, S., Zhang, W., Bai, J., Lu, G., Zhang, L., and Wu, G. (2016c). Construction of a 2D/2D g-C_3N_4/rGO hybrid heterojunction catalyst with outstanding charge separation ability and nitrogen photofixation performance via a surface protonation process. RSC Adv. *6*, 25695–25702.

Hu, S., Chen, X., Li, Q., Li, F., Fan, Z., Wang, H., Wang, Y., Zheng, B., and Wu, G. (2017). Fe^{3+} doping promoted N_2 photofixation ability of honeycombed graphitic carbon nitride: the experimental and density functional theory simulation analysis. Appl. Catal. B *201*, 58–69.

Ileperuma, O.A., Tennakone, K., and Dissanayake, W.D.D.P. (1990). Photocatalytic behavior of metal doped titanium dioxide: studies on the photochemical synthesis of ammonia on magnesium/titania catalyst systems. Appl. Catal. *62*, L1–L5.

Ileperuma, O.A., Thaminimulla, C.T.K., and Kiridena, W.C.B. (1993). Photoreduction of nitrogen to ammonia and water to hydrogen on metal (cerium, vanadium) doped titania catalysts. Sol. Energy Mater. Sol. Cells *28*, 335–343.

Kaufmann, U., Schlotter, P., Obloh, H., Kohler, K., and Maier, M. (2000). Hole conductivity and compensation in epitaxial GaN: Mg layers. Phys. Rev. B *62*, 10867.

Khan, M.M.T., and Rao, N.N. (1990). Photocatalytic hydrogenation of cyclohexene through water as a source of hydrogen by platinum-cadmium sulfide-ruthenium dioxide semiconductor particulate system catalyzed by K$[Ru(H\text{-}EDTA)Cl]_2H_2O$. J. Mol. Catal. *58*, 323–329.

Khan, F., Yue, P., Rizzuti, L., Augugliaro, V., and Brucato, A. (1983). Photoassisted water cleavage and nitrogen fixation over titanium-exchanged zeolites. Ind. Eng. Chem. Prod. Res. Dev. *22*, 238–241.

Kibria, M.G., Nguyen, H.P.T., Cui, K., Zhao, S., Liu, D., Guo, H., Trudeau, M.L., Paradis, S., Hakima, A.-R., and Mi, Z. (2013). One-step overall water splitting under visible light using multiband InGaN/GaN nanowire heterostructures. ACS Nano *7*, 7886–7893.

Kibria, M.G., Chowdhury, F.A., Mi, Z., Qiao, R., Yang, W., Boukahil, I., Himpsel, F.J., Kong, X., Guo, H., Kong, X., et al. (2016). Atomic-scale origin of long-term stability and high performance of p-GaN nanowire arrays for photocatalytic overall pure water splitting. Adv. Mater. *28*, 8388–8397.

Li, Q., Domen, K., Naito, S., Onishi, T., and Tamaru, K. (1983). Photocatalytic synthesis and photodecomposition of ammonia over strontium titanate and barium titanate based catalysts. Chem. Lett. *20*, 321–324.

Li, H., Shang, J., Ai, Z., and Zhang, L. (2015). Efficient visible light nitrogen fixation with biobr nanosheets of oxygen vacancies on the exposed {001} facets. J. Am. Chem. Soc. *137*, 6393–6399.

Li, H., Shang, J., Shi, J., Zhao, K., and Zhang, L. (2016). Facet-dependent solar ammonia synthesis of BiOCl nanosheets via a proton-assisted electron transfer pathway. Nanoscale *8*, 1986–1993.

Li, L., Wang, Y., Vanka, S., Mu, X., Mi, Z., and Li, C.-J. (2017). Nitrogen Photofixation over III-nitride nanowires assisted by ruthenium clusters of low atomicity. Angew. Chem. Int. Ed. *56*, 8701–8705.

Liang, H., Zou, H., and Hu, S. (2017). Preparation of the $W_{18}O_{49}$/g-C_3N_4 heterojunction catalyst with full-spectrum-driven photocatalytic N_2 photofixation ability from the UV to near infrared region. New J. Chem. *41*, 8920–8926.

Liu, J., Kelley, M.S., Wu, W., Banerjee, A., Douvalis, A.P., Wu, J., Zhang, Y., Schatz, G.C., and Kanatzidis, M.G. (2016). Nitrogenase-mimic iron-containing chalcogels for photochemical reduction of dinitrogen to ammonia. Proc. Natl. Acad. Sci. U S A *113*, 5530–5535.

Lu, Y., Yang, Y., Zhang, T., Ge, Z., Chang, H., Xiao, P., Xie, Y., Hua, L., Li, Q., Li, H., et al. (2016). Photoprompted hot electrons from bulk cross-linked graphene materials and their efficient catalysis for atmospheric ammonia synthesis. ACS Nano *10*, 10507–10515.

Maruska, H.P., and Tietjen, J.J. (1969). The preparation and properties of vapor-deposited single-crystal-line GaN. Appl. Phys. Lett. *15*, 327–329.

Miyama, H., Fujii, N., and Nagae, Y. (1980). Heterogeneous photocatalytic synthesis of ammonia from water and nitrogen. Chem. Phys. Lett. *74*, 523–524.

Moustakas, T.D., and Molnar, R.J. (1992). Growth and doping of GaN films by ECR-assisted MBE. MRS Symp. Proc. *281*, 753.

Neugebauer, J., and van de Walle, C.G. (1996). Role of hydrogen in doping of GaN. Appl. Phys. Lett. *28*, 1829.

Newman, N. (1997). The energetics of the GaN MBE reaction: a case study of meta-stable growth. J. Cryst. Growth *178*, 102–112.

Nonomura, S., Kobayashi, S., Gotoh, T., Hirata, S., Ohmori, T., Itoh, T., Nitta, S., and Morigaki, K. (1996). Photoconductive a-GaN prepared by reactive sputtering. J. Non Cryst. Solids *198-200*, 174–177.

Ogden, J.M. (1999). Prospects for building a hydrogen energy infrastructure. Annu. Rev. Energy Environ. *24*, 227–279.

Oshikiri, T., Ueno, K., and Misawa, H. (2014). Plasmon-induced ammonia synthesis through nitrogen photofixation with visible light irradiation. Angew. Chem. Int. Ed. *53*, 9802–9805.

Palczewska, M., Suchanek, B., Dwiłiński, R., Pakua, K., Wagner, A., and Kamińska, M. (1998). Paramagnetic defects in GaN. MRS Internet J. Nitride Semicond. Res. *3*, 45.

Palmisano, L., Augugliaro, V., Sclafani, A., and Schiavello, M. (1988). Activity of chromium-ion-doped titania for the dinitrogen photoreduction to ammonia and for the phenol photodegradation. J. Phys. Chem. *92*, 6710–6713.

Pearton, S.J. (1997). GaN and Related Materials (Gordon and Breach).

Ranjit, K.T., Varadarajan, T.K., and Viswanathan, B. (1996). Photocatalytic reduction of dinitrogen to ammonia over noble-metal-loaded TiO_2. J. Photochem. Photobiol. A *96*, 181–185.

Rusina, O., Eremenko, A., Frank, G., Strunk, H.P., and Kisch, H. (2001). Nitrogen photofixation at nanostructured iron titanate films. Angew. Chem. Int. Ed. *40*, 3993–3995.

Schrauzer, G.N., and Guth, T.D. (1977). Photocatalytic reactions. 1. Photolysis of water and photoreduction of nitrogen on titanium dioxide. J. Am. Chem. Soc. *99*, 7189–7193.

Soria, J., Conesa, J.C., Augugliaro, V., Palmisano, L., Schiavello, M., and Sclafani, A. (1991). Dinitrogen photoreduction to ammonia over titanium dioxide powders doped with ferric ions. J. Phys. Chem. *95*, 274–282.

Sun, S., Li, X., Wang, W., Zhang, L., and Sun, X. (2017). Photocatalytic robust solar energy reduction of dinitrogen to ammonia on ultrathin MoS_2. Appl. Catal. B *200*, 323–329.

Thacker, C.M., Folkins, H.O., and Miller, E.L. (1941). Free Energies of Formation of gaseous hydrocarbons and related substances. Ind. Eng. Chem. *33*, 584–590.

Vitousek, P.M., Aber, J.D., Howarth, R.W., Likens, G.E., Matson, P.A., Schindler, D.W., Schlesinger, W.H., and Tilman, D.G. (1997). Human alteration of the global nitrogen cycle: sources and consequences. Ecol. Appl. *7*, 737–750.

Wang, D., Pierre, A., Kibria, M.G., Cui, K., Han, X., Bevan, K.H., Guo, H., Paradis, S., Hakima, A.-R., and Mi, Z. (2011). Wafer-level photocatalytic water splitting on GaN nanowire arrays grown by molecular beam epitaxy. Nano Lett. *11*, 2353–2357.

Wang, S., Hai, X., Ding, X., Chang, K., Xiang, Y., Meng, X., Yang, Z., Chen, H., and Ye, J. (2017a). Light-switchable oxygen vacancies in ultrafine Bi_5O_7Br nanotubes for boosting solar-driven nitrogen fixation in pure water. Adv. Mater. *29*, 1701774.

Wang, Y., Wei, W., Li, M., Hu, S., Zhang, J., and Feng, R. (2017b). In situ construction of Z-scheme g-C_3N_4/$Mg_{1.1}Al_{0.3}Fe_{0.2}O_{1.7}$ nanorod heterostructures with high N_2 photofixation ability under visible light. RSC Adv. *7*, 18099–18107.

Wu, S., Ross, J.S., Liu, G.-B., Aivazian, G., Jones, A., Fei, Z., Zhu, W., Xiao, D., Yao, W., Cobden, D., and Xu, X. (2013). Electrical tuning of valley magnetic moment through symmetry control in bilayer MoS_2. Nat. Phys. *9*, 149–153.

Xu, Z., Kibria, M.G., AlOtaibi, B., Duchesne, P.N., Besteiro, L.V., Gao, Y., Zhang, Q., Mi, Z., Zhang, P., Govorov, A.O., et al. (2018). Towards enhancing photocatalytic hydrogen generation: which is more important, alloy synergistic effect or plasmonic effect. Appl. Catal. B *221*, 77–85.

Yang, Y., Zhang, T., Ge, Z., Lu, Y., Chang, H., Xiao, P., Zhao, R., Ma, Y., and Chen, Y. (2017). Highly enhanced stability and efficiency for atmospheric ammonia photocatalysis by hot electrons from a graphene composite catalyst with Al_2O_3. Carbon *124*, 72–78.

Zhang, Q., Hu, S., Fan, Z., Liu, D., Zhao, Y., Ma, H., and Li, F. (2016). Preparation of g-C_3N_4/ZnMoCdS hybrid heterojunction catalyst with outstanding nitrogen photofixation performance under visible light via hydrothermal post-treatment. Dalton Trans. *45*, 3497–3505.

Zhao, W., Zhang, J., Zhu, X., Zhang, M., Tang, J., Tan, M., and Wang, Y. (2014). Enhanced nitrogen photofixation on Fe-doped TiO_2 with highly exposed (1 0 1) facets in the presence of ethanol as scavenger. Appl. Catal. B *144*, 468–477.

Zhu, D., Zhang, L., Ruther, R.E., and Hamers, R.J. (2013). Photo-illuminated diamond as a solid-state source of solvated electrons in water for nitrogen reduction. Nat. Mater. *12*, 836–841.

ISCI, Volume *17*

Supplemental Information

Efficient Nitrogen Fixation Catalyzed by Gallium Nitride Nanowire Using Nitrogen and Water

Mingxin Liu, Yichen Wang, Xianghua Kong, Lida Tan, Lu Li, Shaobo Cheng, Gianluigi Botton, Hong Guo, Zetian Mi, and Chao-Jun Li

Supplemental Figures and Tables

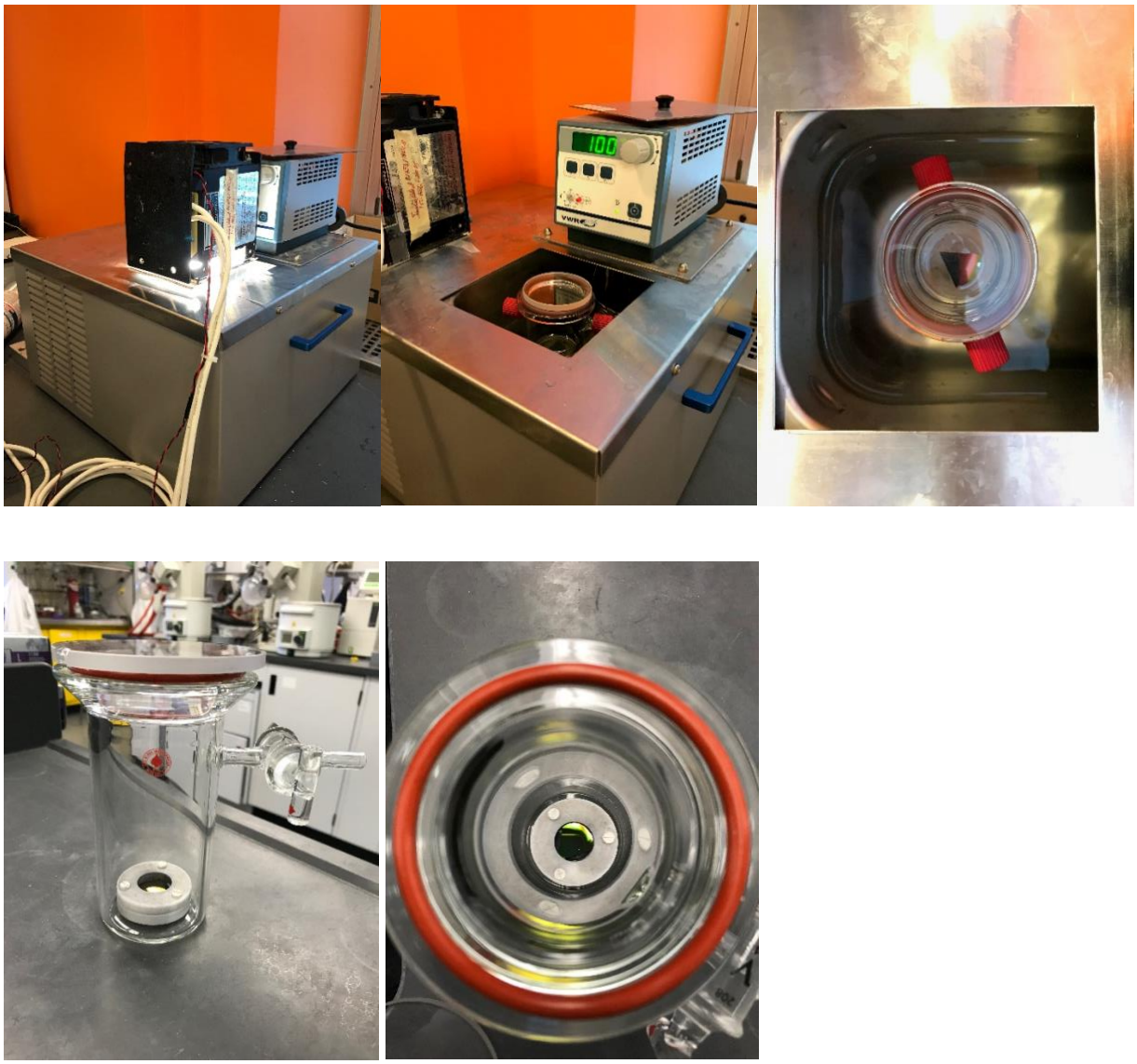

FIGURE S1. Experimental setup for 120 mL quartz chamber (above) and 425 mL quartz chamber (below), Related to Figure 2B-C.

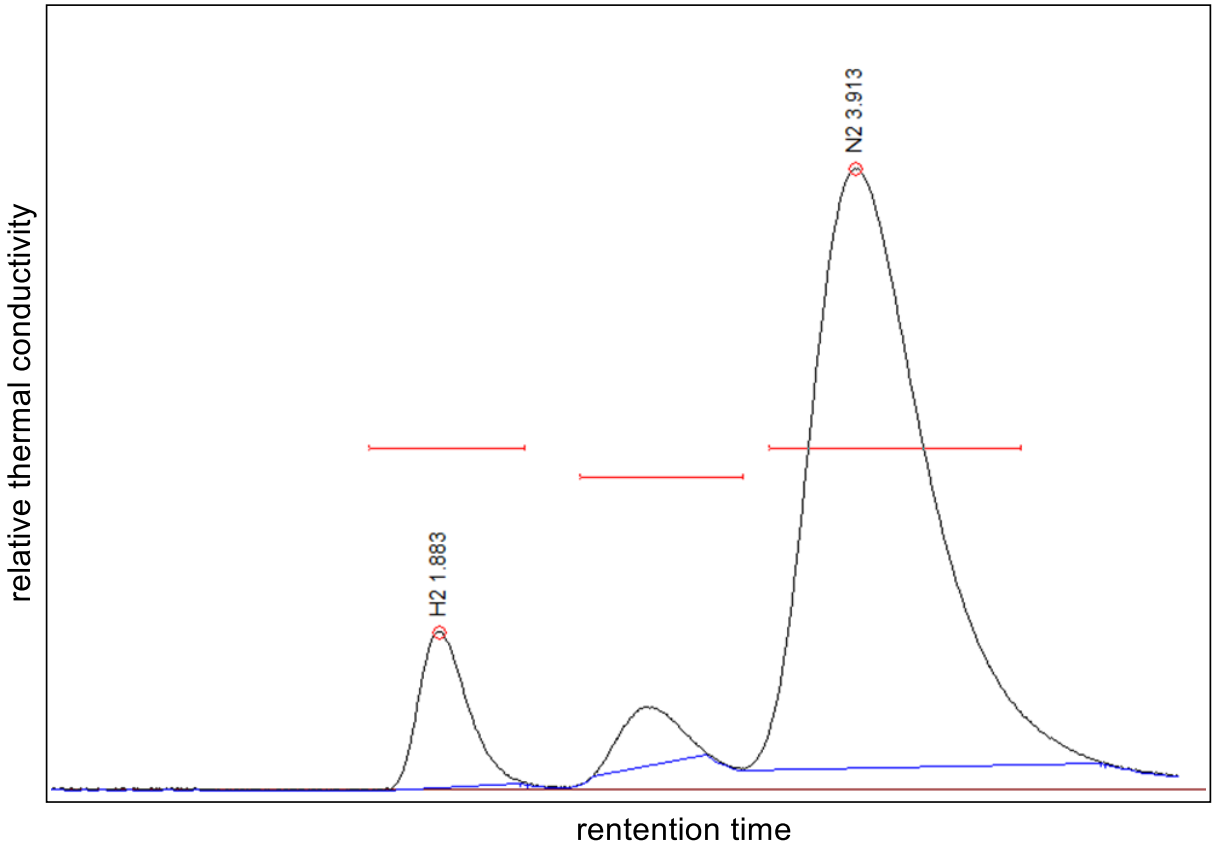

FIGURE S2. A snapshot of GC-TCD peaks during gas sample measurement, showing H_2, N_2 peaks and their retention time (smaller O_2 peak in between was not identified by the instrument), Related to Figure 3B-D.

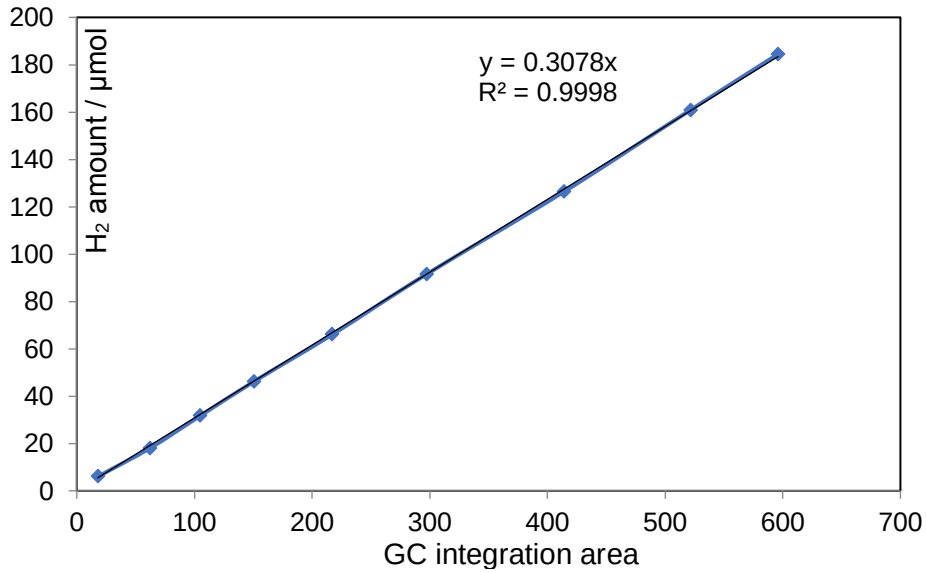

FIGURE S3. H_2 calibration curve (y = H_2 amount in µmol; x = GC peak area), Related to Figure 3B-D.

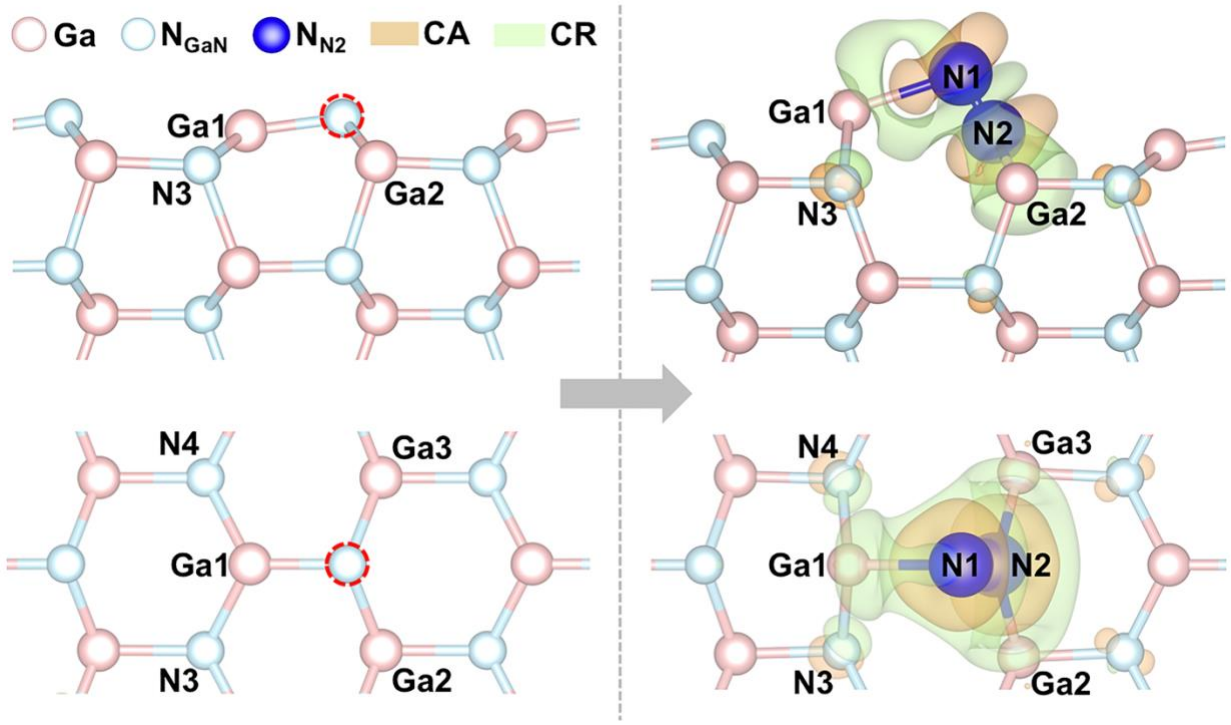

FIGURE S4. Geometric and electronic properties of N_2 adsorption on GaN $(10\bar{1}0)$- wurtzite with N vacancy. Left, top (upper) and side (bottom) view of the fully relaxed atomic structures of GaN $(10\bar{1}0)$-wurtzite. The position of N vacancy is marked with red dashed circle. Right, top (upper) and side (bottom) view of the fully relaxed atomic structures and differential charge density of N_2 adsorption on GaN $(10\bar{1}0)$-wurtzite with N vacancy. CA indicates charge accumulation while CR represents charge reduction. Isosurface contours of electron density differences are drawn at ±0.002 e/Å^3, Related to Figure 1.

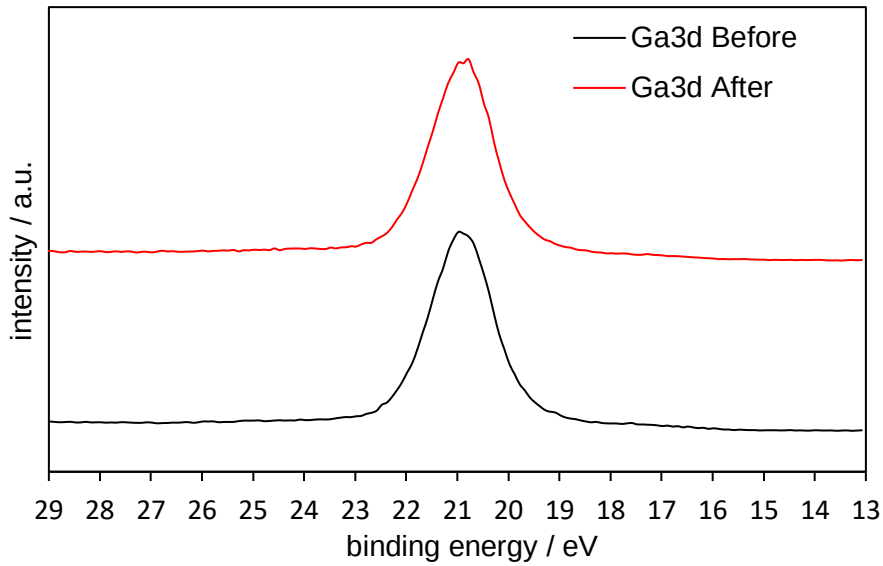

FIGURE S5. XPS Ga^{3d} spectra of the GaN NW before and after N_2 photo-pixation, Related to Figure 2B.

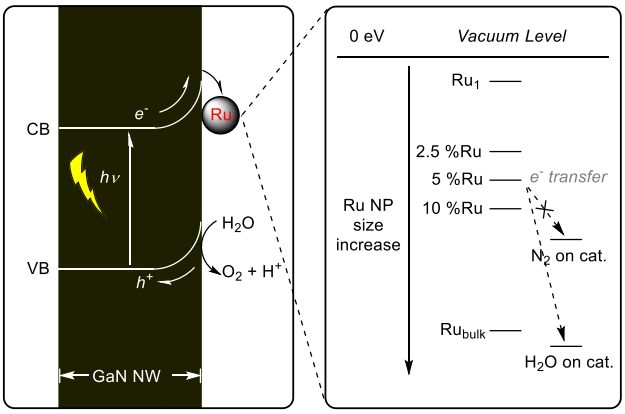

FIGURE S6. Proposed energy diagram for the N_2 fixation vs water-splitting reactivity of Ru@GaN. The electron transfer from Ru to N_2 is less energetically favored compared with to H_2O, Related to Figure 3.

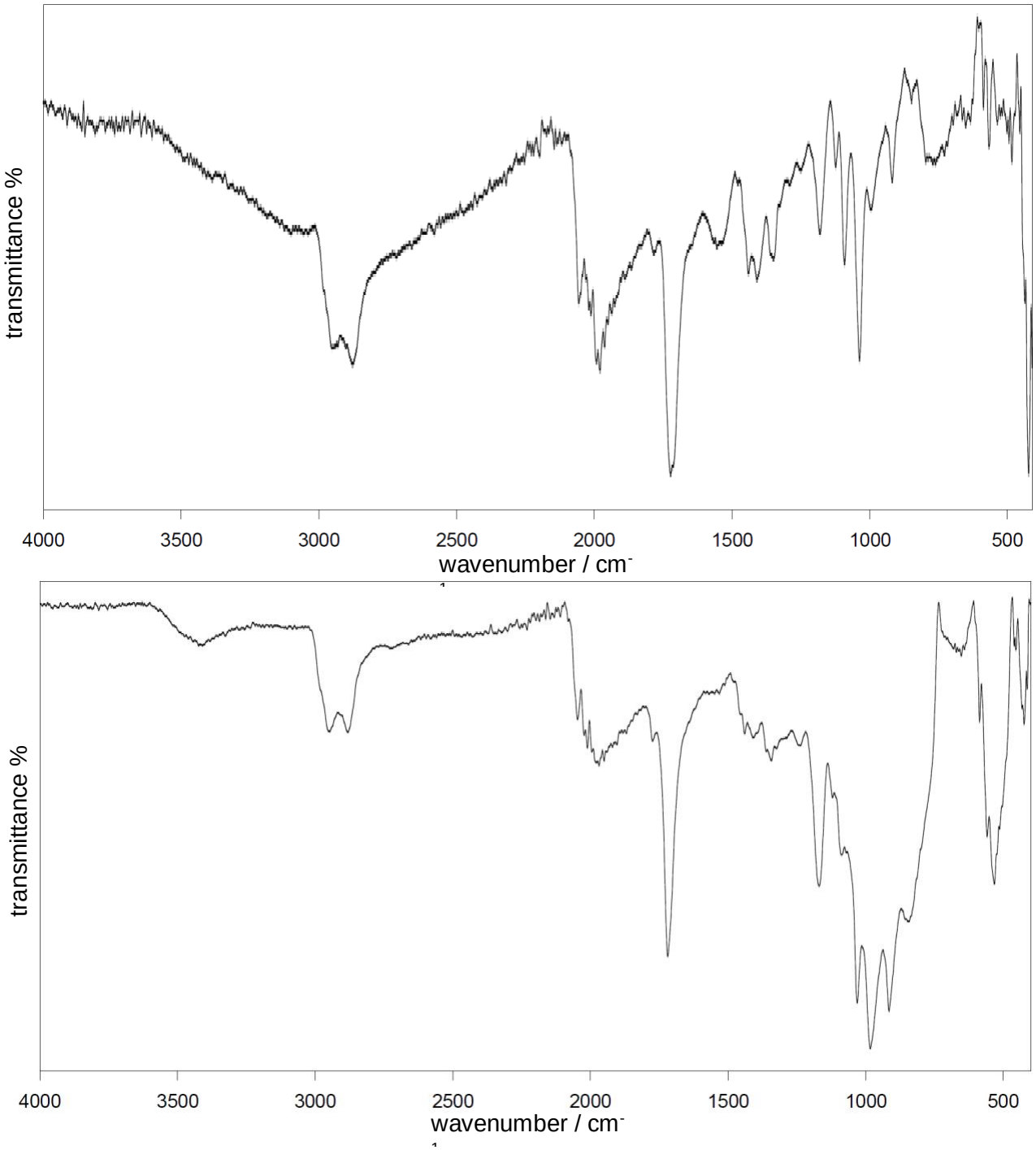

FIGURE S7. IR spectrum of $Ru_3(CO)_{12}$ deposited on TiO_2 (above) and GaN (below), Related to Figure 3H.

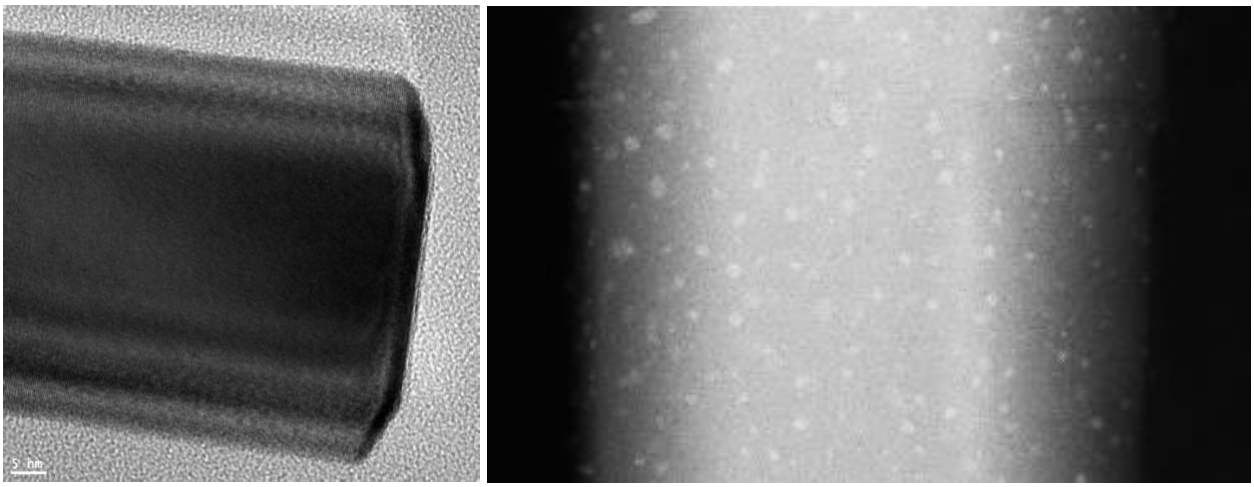

FIGURE S8. TEM image of GaN NW (left) and Ru@GaN NW (right) after photo-reaction, Related to Figure 2B-C and Figure 3B-D.

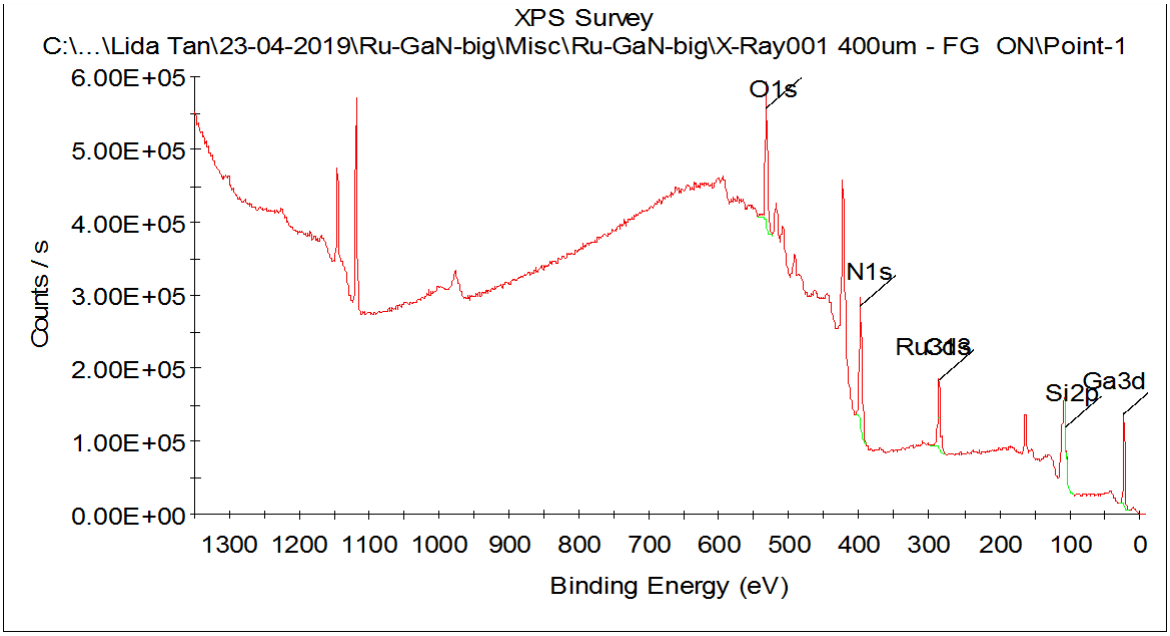

FIGURE S9. XPS full-spectrum of Ru@GaN NW after reaction, Related to Figure 3B-D.

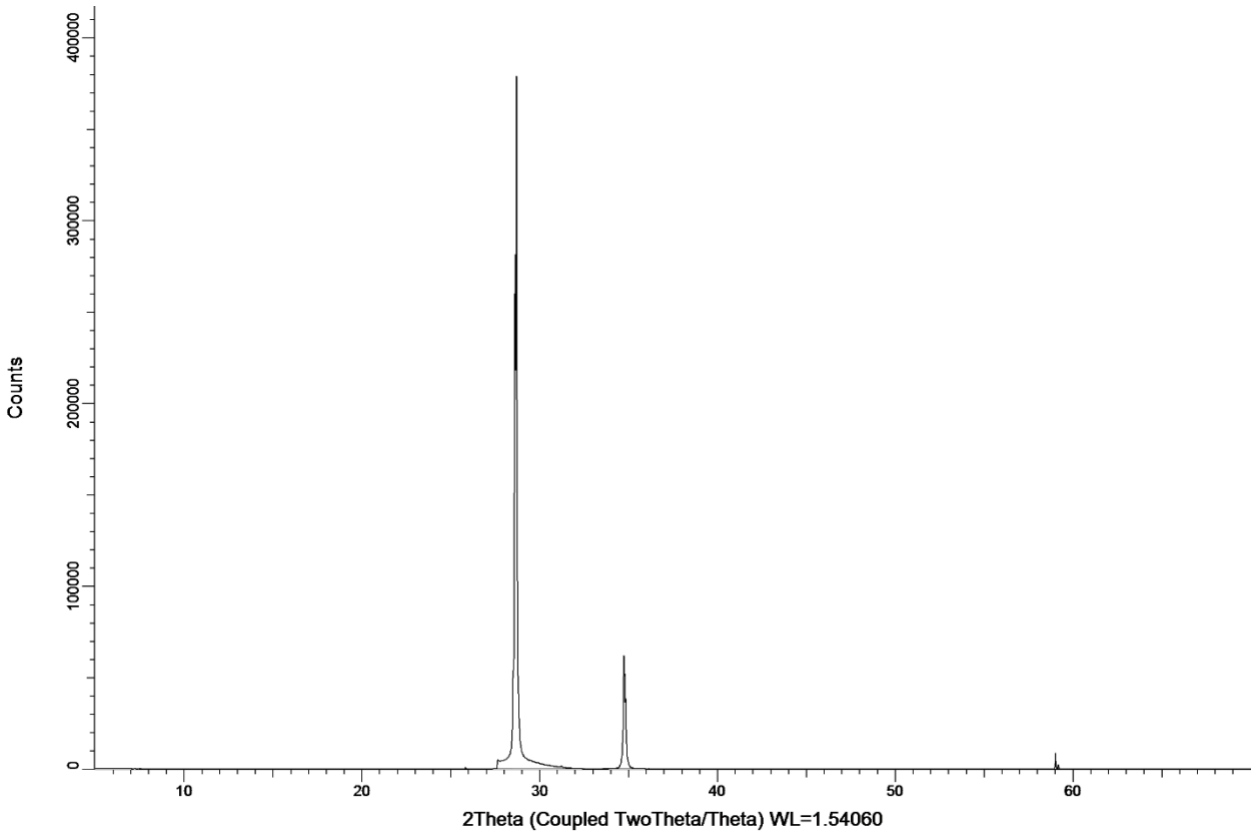

FIGURE S10. XRD spectrum of Ru@GaN NW after photo-reaction, Related to Figure 3B-D.

TABLE S1. Results of the photo-driven N_2 fixation with GaN NW, Related to Figure 2B-C.

Entry	Catalyst[1]	NH_3 yield ($\mu mol \cdot g_{cat}^{-1} \cdot h^{-1}$)
1	p-GaN NW	190
2	i-GaN NW	310
3	n-GaN NW	450
4	GaN Powder	170
5	Si(111) Wafer	not detected
6	n-GaN[2]	Not detected
7	n-GaN[3]	Not detected
8	n-InGaN/GaN[3]	340
9	n-GaN[4]	491
10	n-GaN (2^{nd} cycle)	462
11	n-GaN (3^{rd} cycle)	453
12	n-GaN (4^{th} cycle)	453
13	n-GaN (5^{th} cycle)	450
14	n-GaN (6^{th} cycle)	446
15	n-GaN (7^{th} cycle)	438
16	n-GaN (8^{th} cycle)	444
17	n-GaN (9^{th} cycle)	433
18	n-GaN (10^{th} cycle)	429
19	n-GaN (11^{st} cycle)	430
20	n-GaN (12^{nd} cycle)	425
21	n-GaN (13^{rd} cycle)	420

[1]: Reaction condition: 425 mL quartz chamber, 16 mmol N_2, 1.5 mL H_2O, react for 1 h.
[2]: Reaction was conducted without N_2.
[3]: > 400 nm long pass light filter was applied to the light source.
[4]: Reaction was conducted for 12 h.

TABLE S2. Results of the photo-driven simultaneous N_2 fixation and water-splitting with Ru@GaN NW, Related to Figure 3B-D.

Entry	Catalyst[1]	NH_3 yield ($\mu mol \cdot g_{cat}^{-1} \cdot h^{-1}$)	H_2 yield ($\mu mol \cdot g_{cat}^{-1} \cdot h^{-1}$)	O2 yield ($\mu mol \cdot g_{cat}^{-1} \cdot h^{-1}$)
1	5%Ru@p-GaN NW	39	not detected	not detected
2	5%Ru@i-GaN NW	121	71	90
3	5%Ru@n-GaN NW	182	283	230
4	n-GaN NW	452	trace	trace
5	GaN Powder	171	not detected	not detected
6	Si(111) Wafer	not detected	not detected	not detected
7	5%Ru@Si(111) Wafer	not detected	not detected	not detected
8	5%Ru@n-GaN NW[2]	not detected	not detected	not detected
9	5%Ru@n-InGaN NW[2]	86	not detected	not detected
10	2.5%Ru@n-GaN NW	101	not detected	not detected
11	10%Ru@n-GaN NW	38	132	80
13	5%Ru@n-GaN NW[3]	290	99	240
14	5%Ru@n-GaN NW[4]	468	trace	trace

[1]: Reaction condition: 425 mL quartz chamber, 16 mmol N_2, 1.5 mL H_2O, react for 1 h.
[2]: > 400 nm long pass light filter was applied to the light source.
[3]: Reaction was conducted at 50 °C.
[4]: Reaction was conducted at 90 °C.

TABLE S3. Geometry parameters, Bader charge analysis of N_2 adsorption on pristine m-plane of GaN nanowires and m-plane of GaN nanowires with N vacancy compared to N_2 in its isolated gas phase, Related to Figure 1.

Species	Bond length (Å)		Bader Charge Variation (e)		
	N1-N2	Ga1-N3/N4	N_1	N_2	Total
N_2	1.11	-	-	-	-
Pristine m-plane of GaN	1.11	1.91	0	0	0
m-plane of GaN with N vacancy	1.25	2.09	0.2447	0.7400	0.9847
	1.28	2.01	0.7582	0.3498	1.1080

Transparent Methods

1. Growth of GaN and InGaN/GaN Nanowires.

The catalyst-free GaN and InGaN/GaN nanowires are grown on a Si (111) wafer using radio frequency plasma-assisted molecular beam epitaxy (MBE) in nitrogen rich conditions. The Si substrates were cleaned in clean room by absolute methanol, acetone, and essentially hydrofluoric acid prior of loading into the MBE system. Growth conditions: temperature ~750 ^{o}C, nitrogen flow rate 1 sccm, forward plasma power ~400 W. The as-synthesized nanowires can be doped with tetravalent (Si^{4+}) or divalent (Mg^{2+}) ions for making n- and p- type semiconductors, respectively. The doping density is controlled by tuning the effusion cell temperatures of Ge Mg and In. For n-type doping, the Ge effusion cell temperature is 1100 °C. For p-type doping, the Mg effusion cell temperature is 265 °C. For the incorporation of indium, the indium effusion cell temperature is varied from 705 ^{o}C to 795 ^{o}C. The electron and hole concentrations for the Ge-doped n-type and Mg-doped p-type GaN NWs were estimated to be on the order of $n = 5 \times 10^{18}$ cm^{-3} and $p = 1 \times 10^{18}$ cm^{-3}, respectively. Other growth parameters were kept constant.

2. The deposition of Ru co-catalyst.

Ruthenium loading was conducted via the impregnation of as-synthesized GaN NWs (0.35 mg) with a solution of $Ru_3(CO)_{12}$ in dry THF (1.5 mL), followed by the complete loss of carbonyl groups in vacuum under a temperature program of 2 ^{o}C min^{-1} up to 200 ^{o}C, held for one hour, then 1 ^{o}C min^{-1} up to 350 ^{o}C, held for two hours and then cooled to ambient temperature. The Ru content was further confirmed by using the XPS measurement before and after the decomposition process.

3. Photo-driven N_2 fixation.

A slice of freshly-prepared GaN catalyst (equivalent to 0.35 mg GaN) was placed at the bottom of an airtight quartz reactor equipped with a vacuum hose (a holder was used to anchor the catalyst

and keep it under the light, see Figure S1 in Supplementary Information) with 1.5 mL distilled water added. The reactor (vol. 425 mL) was then frozen by liquid nitrogen, pumped down by oil pump, and thawed by warm water bath (Freeze-Pump-Thaw degassing, repeated for 5 cycles). 16 mmol of Ultra-High-Purity (UHP, 99.999 %) grade N_2 was then flushed into the reactor. The reactor was then partially submerged in a 25 ^oC chiller and illuminated by a 300w full-arch Xe lamp for 1 h. After illumination, the presence of ammonia was confirmed by both GC-MS and salicylate test using the reaction mixture in the reactor followed by colorimetric quantification using UV-Vis spectroscopy[1].

4. N_2 fixation by Ru@GaN.

A slice of freshly-prepared Ru@GaN catalyst (equivalent to 0.35 mg GaN) was placed directly at the bottom of an airtight quartz reactor containing 1.5 mL distilled water. The reactor (vol. 425 mL) was evacuated completely (Freeze-Pump-Thaw degassing, repeated for 5 cycles) before 16 mmol of Ultra-High-Purity (UHP, 99.999 %) grade N_2 was injected. The reactor was then partially submerged in a 10 ^oC chiller and illuminated by a 300w full-arch Xe lamp for 1 h. After illumination, the gas phase of the reactor was directly injected into gas chromatography (GC) equipped with a thermal conductivity analyzer to identify the gas product. The presence of ammonia was confirmed by both GC-MS and salicylate test using the reaction mixture in the reactor followed by colorimetric quantification using UV-Vis spectroscopy[1].

4. General Characterization.

Scanning electron microscopy (SEM) images were recorded using Zeiss Nvision equipped with InLens detector at 5 kV. High resolution transmission electron microscope (TEM) images were obtained using FEI Titan HB at accelerating voltage of 200 kV and 100 pA beam current. The UV-vis absorption spectra were measured with a Shimadzu UV-2450 spectrophotometer. The X-ray photoelectron spectroscopy (XPS) was

performed on an ESCALAB 250 X-ray photoelectron spectrometer with a monochromated X-ray source (Al Kαhυ= 1486.6 eV). The energy scale of the spectrometer was calibrated using Au 4f7/2, Cu 2p3/2, and Ag 3d5/2 peak positions. The standard deviation for the binding energy (BE) values was 0.1 eV. Gas Chromatography (GC) was measured using Shimazu GC-8A Gas Chromatography. Infrared (IR) Spectrum was measured directly using powder sample by Bruker ALPHA FT-IR Spectrometer. NMR spectrum obtained in the isotope labeling experiment was measured by Bruker Ascend^{TM} 500MHz using solvent suppression mode for 20000 scans. The identification of $^{15}NH_3$ and $^{14}NH_3$ was according to their different splitting pattern and coupling constant.[2, 3] EPR study was conducted on Bruker Elexsys 580 FT/CW EPR Console.

5. Density functional theory calculation

Density functional theory calculations were performed using the generalized gradient approximation for the exchange-correlation potential, the projector augmented wave method[4-5] and a plane-wave basis set as implemented in the Vienna ab-initio simulation package.[6] The energy cut-off for the plane-wave basis was set to 600 eV for all relaxation, energy and electronic properties calculations. Two k-meshes of 3×3×1 and 4×4×1 and were adopted to relax and static calculations, separately, and the mesh density of k points was kept fixed when performing related calculations with primitive cells. In optimizing the system geometry, van der Waals (vdW) interactions were considered by the vdW-DF level with the optB86 exchange functional (optB86-vdW).[7-8] For the calculation of N_2 adsorption on the GaN surface, six layers of Ga and N atoms and a 5 × 3 supercell were used. The molecule was put on one side of the slab with two different kinds of pseudo hydrogen atoms passivating the dangling bonds at the bottom of the slab. A dipole correction was made to get rid of the spurious interaction owing to the presence of non-equivalent surfaces.[9-10] Calculations were performed with applying spin-polarization. All atoms except the bottom three layers were fully relaxed until the net force per atom was less than 0.001 eV·Å^{-1}.

Differential Charge Density (DCD) was adopted to qualitatively evaluate the charge density difference $\Delta\rho(r)$, which can be defined as follows,

$$\Delta\rho(r) = \rho_{ads+sub}(r) - \rho_{ads}(r) - \rho_{sub}(r), \quad (1)$$

where $\rho_{ads+sub}(r)$ represents the total charge density of the fully relaxed configuration of N_2 adsorption on GaN surface. $\rho_{ads}(r)$ and $\rho_{sub}(r)$ are the total electronic charge densities of the separated N_2 and GaN surfaces, respectively, which maintain the same geometrical structures as in the relaxed N_2 adsorption system. Accordingly, a positive or negative sign $\Delta\rho(r)$ can be used as an indication of whether the charges at that site are increasing or depleting.

6. Quantum efficiency calculation

Quantum efficiency is calculated based on the number of ammonia molecule generated and the photon absorbed per hour. Due to the presence of water on GaN surface, the reflection co-efficient of GaN, water, and the total number of photons between 200-365nm need to be considered. Based on the assumption in our previous study[11], the corresponding photon number on the size of our catalyst (approx. 2.8 cm^2) equals 1×10^{18} s^{-1}. Therefore, the estimated quantum efficiency QE ≈ 10 %.

Supplemental References

1. Li, L.; Wang, Y.; Vanka, S.; Mu, X.; Mi Z.; Li, C.-J. *Angew. Chem. Int. Ed.* **2017**, *56*, 8701-8705.
2. Liu, J.; Kelley, M. S.; Wu, W.; Banerjee, A.; Douvalis, A. P.; Wu, J.; Zhang, Y.; Schatz G. C.; Kanatzidis, M. G. *Proc. Natl. Acad. Sci. U. S. A.* **2016**, *113*, 5530-5535.
3. Zhou, F.; Azofra, L. M.; Ali, M.; Kar, M.; Simonov, A. N.; McDonnell-Worth, C.; Sun, C.; Zhang X.; MacFarlane, D. R. *Energy Environ. Sci.* **2017**, *10*, 2516-2520.

4 Blochl, P. E. *Phys. Rev. B* **1994**, *50*, 17953-17979.

5 Kresse, G.; Joubert, D. *Phys. Rev. B* **1999**, *59*, 1758-1775.

6 Kresse, G.; Furthmuller, J. *Phys. Rev. B* **1996**, *54*, 11169-11186.

7 Klimes, J.; Bowler, D. R.; Michaelides, A. *Phys. Rev. B* **2011**, *83*, 195131.

8 Klimes, J.; Bowler, D. R.; Michaelides, A. *J. Phys-Condens Mat.* **2010**, *22*, 022201.

9 Neugebauer, J; Scheffler, M. *Phys. Rev. B* **1992**, *46*, 16067-16080.

10 Makov, G.; Payne, M. C. *Phys. Rev. B* **1995**, *51*, 4014-4022.

11 Kibria, M. G.; Zhao, S.; Chowdhury, F. A.; Wang, Q.; Nguyen, H. P. T.; Trudeau, M. L.; Guo, H.; Mi, Z. *Nat. Commun.* **2014**, *5*, 3825.